Radio Propagation Measurement and Characterization in Outdoor Tall Food Grass Agriculture Field for Wireless Sensor Network at 2.4 GHz Band

Tossaporn Srisooksai[1, *], Kamol Kaemarungsi[2], Junichi Takada[3], and Kentaro Saito[3]

Abstract—This paper describes the radio propagation measurement campaign in a sugarcane field representing a tall food grass characteristic which is one of the common types of outdoor agriculture environments. The measurement was conducted by using a channel sounder having a bandwidth of 45.6 MHz at 2.45 GHz with the aim of investigating the propagation channel characteristics which are useful in deploying wireless sensor networks in precision agriculture. By analogy with the Ikegami model, the variation of the path loss over the relative angles between the plant rows and the line-of-sight direction from the transmitter to the receiver is identified. Utilizing this knowledge, this work justifies the procedure of predicting the path loss at any point in the field by a few measurement efforts. Furthermore, the Rician K-factor and root-mean-square delay spread are investigated for vegetation depths less than 40 m. The result shows that the relationship between the Rician K-factor and its corresponding path loss value in each measurement point can be fitted with the log-linear line. This leads to the possibility of predicting the K-factor at any point in the field. In addition, because the result of the root-mean-square delay spread is independent of the vegetation depth and the density of the plant, it is represented by the statistical model in which the Weibull distribution provides the best representation.

1. INTRODUCTION

Precision agriculture is the management of the spatial and temporal variability of agriculture fields using information, communication, and technology [1]. Wireless sensor network (WSN), which is a combination of sensor nodes and a wireless network, plays a significant role in gathering such variability in the fields so that precision management can be applied to obtain the maximum yield. For the gathering application, numerous sensor nodes are scattered around a wide geographical area in which two significant requirements are crucial: the reliability of wireless communication in terms of network coverage [2] and low energy consumption for maximizing the wireless network's lifetime [3]. In [2, 4], the authors showed that knowledge of radio propagation channel parameters such as path loss and small-scale fading helps achieve these requirements.

Several existing works [5–11] have investigated radio propagation in the forest. The path loss was modeled empirically in [7, 8]. More microscopic radio propagation characteristics such as the shadowing loss [9] and small-scale fading [5, 6, 9, 10] for narrow-band channels as well as the characteristics of ultra-wideband (UWB) channels [12] were modeled empirically.

Such empirical models in the forest environment give many useful insights for radio propagation in agriculture fields, and some parameters of the propagation channel might be applicable to fruit orchards

because they are also dominated by trees with a single trunk. However, it might be problematic for the case of tall food grass — the Poaceae family in botanical terminology [13] such as corn and sugarcane — as well as the case of herb fields. Recently, the authors of [14] empirically fitted the measurement results from a corn field at 2.4 GHz by using the model's parameters recommended for the forest case. The underprediction result of the path loss is shown, especially during the crop maturity stage.

Recently, measurements in various types of outdoor agriculture fields for various frequencies and different antenna heights were conducted [2, 14–16]. In [2], the path loss results using antenna heights of 0.15 m and 1 m were compared in the cashew orchard, corn field, and herb field at 2.4 GHz band. Although the measurements using an antenna height at 0.15 m showed greater path loss in all the fields, the path loss difference between the two antenna cases is dependent on the relative of the antenna height and the plant height. In the cashew orchard and corn field where the plant height is higher than 1 m, the difference is small, $\approx$ 3–7 dB at 10 m of vegetation depth. In the herb case, where the plant height is higher than 0.15 m but lower than 1 m, the difference is significantly large, $\approx$ 20 dB at 10 m of vegetation depth. In [14, 16], the effect of the plant height on the path loss was investigated. The antenna height was fixed, and the path loss at every 0.15 m change in mulberry tree height was investigated in 920 MHz band in [16]. In tall food grass type, the path loss of two different corn heights was studied in 2.4 GHz band in [14]. Both works pointed out that the path loss is dependent on the plant height, the loss being greater when the plants are taller. The effect of antenna polarization was studied in the mulberry orchard in [16], which pointed out that the horizontal polarization was less affected by the plants than the vertical polarization.

Because the trees in forests are randomly distributed while the plants in agriculture fields are regularly planted in rows/ridges, another environmental factor causing a significant path loss difference in agriculture fields is the relative angle between the plant rows and the line-of-sight (LOS) direction from the transmitting antenna (Tx) to the receiving antenna (Rx). In [15], two cases of this factor were investigated in mango and oil palm orchards: the LOS direction was between two rows of trees (0°) and the plant rows coinciding with the LOS direction (90°). In the tall food grass type, only the plant rows coinciding with the LOS direction (90°) were studied in [2, 14].

In addition to the path loss, small-scale fading for the agriculture case has not been reported yet in existing works. Although investigations of the small-scale fading in forest scenarios were well represented by the Rician K-factor [6, 9], the distance of radio communication used in those measurements was longer than 40 m which is not a suitable range for precision agriculture [17]. Furthermore, because low data rate transmission uses narrow bandwidth of the WSN, wideband propagation channel parameters are not necessary, and they have not been studied by the existing works. However, recently several proposals have emerged which apply multimedia sensor networks and computer vision techniques to analyze the plant and field conditions in agriculture [18–20]. More bandwidth for data transmission will be ultimately needed for implementing such techniques in the future.

In comparison with the existing studies mentioned above, the original contribution of this paper can be summarized as follows. First, the influence of the tall food grass crop, which is one of the common types of outdoor agriculture environments, on the radio channel propagation characteristics is clarified through measurements in a sugarcane field. The results in the 2.4 GHz band are reported in this work because it has a higher theoretical propagation loss, and thus it is more difficult to manage the radio coverage than in other lower frequency bands applied in the WSN such as 868 and 920 MHz, although it is able to provide higher data transmission [21]. Second, the effect of the relative angle between the plant rows and the LOS direction from the Tx to Rx on the path loss has been comprehensively investigated. The results reveal that the number of ridges existing between the LOS of the Tx and Rx is the dominant cause of the angular variation. Therefore, the vegetation obstruction (VO) model is proposed to better represent the angular variation. Utilizing the proposed model, the procedure of predicting the path loss at any point in the sugarcane field by using a few measurement results can be formulated. Although further experimental validation is needed, the same procedure is expected to be applicable to other food grass agriculture fields under the conditions described in this work. This procedure can reduce much of the effort in practical WSN planning and deployment. Third, the small-scale fading in terms of the Rician K-factor is investigated for a range of vegetation depth that is more suitable for precision agriculture than the existing works. It reveals the possibility of predicting the Ricain K-factor at any point in the field if the path loss information is available. Finally, due to lack of wideband channel

parameters in the tall food grass scenario, the root-mean-square (RMS) delay spread is investigated in this work. This information will be useful for designing the high data rate communication which might be needed in future systems.

The rest of this paper is organized as follows. The existing channel modeling approaches in vegetation environment are reviewed in Section 2. The measurement campaign is described in Section 3. The data processing of estimating the channel parameters is given in Section 4. The difference between the modeling approaches used in this work and the existing works is highlighted in Section 5. In Section 6, the angular variation of the path loss and the prediction of the path loss at any point in the field are discussed. The Rician K-factor and RMS delay spread parameters are characterized in Section 7 and Section 8, respectively. Finally, the conclusions are given in Section 9.

2. EXISTING MODELING APPROACHES

2.1. Path Loss Modeling

In the existing works for both forest and agriculture environments, the path loss $L_{\mathrm{L}}(d_{\mathrm{t}})$ is typically modeled [9, 11, 16] as

$$L_{\mathrm{L}}(d_{\mathrm{t}}) = L_{\mathrm{F}}(d_{\mathrm{t}}) + L_{\mathrm{E}}(d), \ \mathrm{dB} \tag{1}$$

where d_{f} is the distance from the Tx located outside the vegetation area to the interface of the vegetation area, d_{t} the distance between the Tx and Rx, and $d = d_{\mathrm{t}} - d_{\mathrm{f}}$ the vegetation depth as illustrated in Fig. 1. L_{E} is the vegetation attenuation model of the excess loss E, which is generally defined as the path loss value L that exceeds the free space path loss L_{F} as

$$E(d) = L(d_{\mathrm{t}}) - L_F(d_{\mathrm{t}}). \ \mathrm{dB} \tag{2}$$

For clarity, it is emphasized that the path loss value L and excess loss value E are obtained from the measurement, whereas L_{L} and L_{E} are used to represent the models of L and E, respectively. Comprehensive details of such vegetation attenuation models, which are classified into analytical and empirical models, are presented in [22]. A brief summary is given here for completeness.
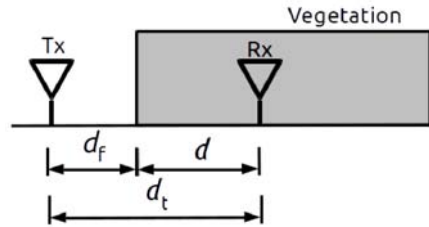

Figure 1. Definition of the vegetation depth (d).

2.1.1. Analytical Model

The analytical model based on the theory of radiative energy transfer (RET) is derived in [23]. In this model, L_{E} is the result of the interplay between the coherent and incoherent components of the electromagnetic field in a random medium of vegetation scatterers. The coherent component is the average field which has a well-defined direction and polarization of propagation. This part decreases due to both absorption and scattering with high attenuation rates and dominates at short distances from the electromagnetic source. The incoherent component is the zero-mean field and is generated by the scattering of the coherent component. Thus, it consists of many waves propagating in various directions. This part dominates at large distances from the source, resulting in a reduced attenuation rate. Therefore, this model exhibits two slopes (gradients) of the ratio between the excess loss E and vegetation depth d: the large gradient at shorter d and the small gradient at large d.

2.1.2. Empirical Model

The widely accepted empirical generic models for the excess loss E are the modified exponential decay (MED) model and the modified gradient model. Although the equation forms of the models are different, their common feature is that they can be used to represent two gradients of the attenuation rate described previously.

The MED model which is sometime known as COST 235 model [24] is expressed as

$$L_{\text{Emed}}(d) = U f^V d^W \text{ dB} \tag{3}$$

where f is the frequency, and U, V, and W are the fitting parameters.

As mentioned in [25], the modified gradient model was intentionally proposed to represent two gradients of the attenuation rate observed through the measurements in which the initial gradient of the attenuation increases rapidly over shorter vegetation depths d, after which the final gradient of the attenuation is considerably slower at large d. Such behavior is in agreement with the analytical-model-based RET described previously. There are two models in this group: the maximum attenuation (MA) model and the non-zero gradient (NZG) model [25] described as Eqs. (4) and (5), respectively:

$$L_{\text{Ema}}(d) = A_{\text{m}} \left\{ 1 - \exp\left(-\frac{R_0}{A_{\text{m}}} d \right) \right\}, \text{ dB} \tag{4}$$

$$L_{\text{Enzg}}(d) = R_\infty d + M \left\{ 1 - \exp\left(-\frac{R_0 - R_\infty}{M} d \right) \right\}. \text{ dB} \tag{5}$$

In these models, R_0 (dB/m) and R_∞ (dB/m) represent the initial and final gradients of the attenuation rate of E, respectively. Originally, A_{m} (dB) in Eq. (4) and M (dB) in Eq. (5) represent the maximum and the offset of E, respectively. However, when R_∞ in Eq. (5) approaches zero, M in Eq. (5) $\approx A_{\text{m}}$ in Eq. (4), and thus the NZG model becomes the MA model. This MA form has been recently used to represent the ITU-R model for the terrestrial path with one terminal in forest/woodland [11].

2.2. Model Selection

In the existing works [2, 14–16, 26, 27], the common way of determining the best L_{E} model for the samples of the excess loss E is to use the least squares model fitting in which the model giving the lowest root-mean-square error (RMSE) is selected. However, the drawback is that the fitting error is easily reduced by increasing the number of model parameters m.

2.3. Small-Scale Fading Modeling

Modeling small-scale fading is to explain the superposition (or unresolved components) of the multipath components with the statistical distribution function [28]. In the forest scenario, where the measurements were conducted at $d > 40$ m [6, 9], such fading is found to be well modeled by the K-factor of the Nakagami-Rice distribution. Furthermore, the linear relationship between the Rician K-factor and d was reported in [6] and the linear relationship between the Rician K-factor and $\log_{10}(d)$ known as the *log-linear* model was reported in [9].

2.4. Wideband Characteristic Modeling

The RMS delay spread, τ_{rms}, is an essential parameter that needs to be characterized in designing a wideband communication system and represents the delay dispersion of the channel [29]. In the existing work on the UWB measurement in the forest environment [12], in the case of $d > 40$ m, τ_{rms} clearly dominates d; τ_{rms} is greater when d is larger. However, this tendency cannot be clearly observed at $d < 40$ m, especially in the dense forest.

3. MEASUREMENT CAMPAIGN

The measurement of the propagation channel in the sugarcane field was conducted in the rural area of Chonburi province located in the east of Thailand during October 17–27, 2017. The measurement

Table 1. Channel sounding parameters.

Parameters	Value
Center frequency	2.45 GHz
Number of frequency tones	134
Total bandwidth	45.6 MHz
Frequency tone spacing	343 kHz
Symbol duration	2.9 µs
Delay resolution	21.9 ns
Total measurement time	0.5 s
Antenna	Directional outdoor WiFi antenna
for both Tx and Rx.	Vertical polarization
	Vertical beamwidth: 30°
	Horizontal beamwidth: 30°
	Gain: 14 dBi
	Height: 1.7 m

was conducted by using a channel sounder that was specifically designed and developed in [30] for the outdoor agriculture environment. The important parameters of the channel sounder used in the measurement are summarized in Table 1. The Tx antenna was fixed at a certain point while the Rx antenna was moved to the specific points and angular directions in the field manually. It takes 0.5 s for one snapshot of the measurement and the time-invariant condition is assumed due to lack of dynamic movement during the period. A preliminary measurement was also conducted to ensure that there was no radio signal interference from other radio transmission systems.

The area of the sugarcane field is $50 \times 40 \, \text{m}^2$. The sugarcane plant is ten months old with an average height of 3.5 m as shown in Fig. 2. The range of the cane diameters is 0.03–0.04 m. The ridge width is 0.15 m and the canes stand close to each other in each ridge. The crop cycle of the sugarcane is approximately 11 months and the height is up to 4 m. Therefore, the radio prorogation result obtained from this scenario is close to the most severe case. The antenna height was set at 1.7 m which is the same as the height used in the real implementation in [31]. In addition, the effect of the relative angle between the plant ridges and the LOS direction from the Tx to the Rx defined as ϕ on the path loss was investigated. As shown in Fig. 3, the case in which the LOS direction is between two ridges of the
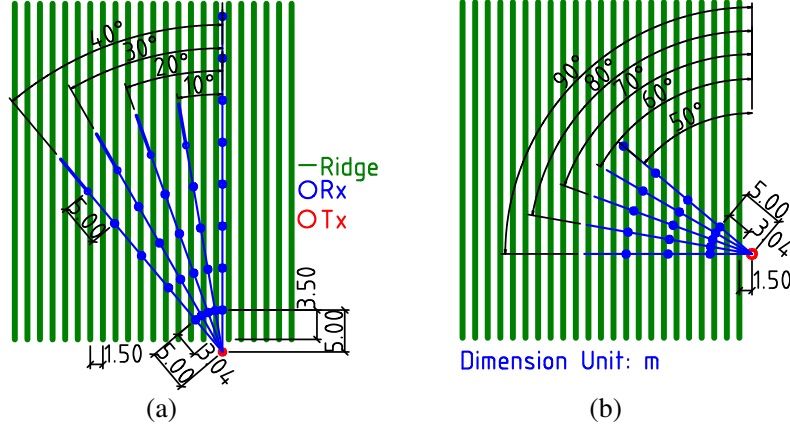

Figure 2. Measurement in the sugarcane field.

Figure 3. Measurement in the sugarcane field. (a) Measurement cases from $\phi = 0°$ to $40°$. (b) Measurement cases from $\phi = 50°$ to $90°$.

sugarcane is defined as $\phi = 0°$. In each ϕ direction, the Tx is placed outside the field, and the Rx is moved with 5 m steps in the field. The Tx and Rx antennas were oriented for a maximum response. The same process is repeated for the other angles.

4. DATA PROCESSING

The data processing involved in the path loss value estimation is first described. Then, the estimation of the RMS delay spread is explained in Section 4.2 because the condition used to estimate this parameter is also used to estimate the coherence bandwidth which will later be utilized to estimate the Rician K-factor of the small-scale fading in Section 4.4.

4.1. Path Loss Estimation

The output of the channel sounder is the 45.6 MHz bandwidth channel transfer function $H[t, k]$ of each measurement point represented by d_t and ϕ defined in Figs. 1 and 3, where $k = 1, 2, \ldots, K$ denotes the frequency index, K the number of frequency tones shown in Table 1, $t = 1, 2, \ldots, T$ the snapshot index, and a snapshot duration equals a symbol duration, as shown in Table 1. Then the Tx antenna gain g_{Tx} and Rx antenna gain g_{Rx} are eliminated as

$$\hat{H}[t, k] = \frac{H[t, k]}{\sqrt{g_{\mathrm{Tx}} g_{\mathrm{Rx}}}}. \tag{6}$$

The average path gain value G of each measurement point can be obtained by averaging the power of $\hat{H}[t, k]$ over k and t as

$$G = \frac{1}{KT} \sum_{t=1}^{T} \sum_{k=1}^{K} |\hat{H}[t, k]|^2. \tag{7}$$

This average is applied in order to remove the small-scale fading due to the superposition of the multipath components. This fluctuation will be modeled later by the Rician K-factor. Then, the path loss value L of each measurement point, which is the inverse path gain ratio, is estimated as

$$L = 10 \cdot \log_{10}\left(\frac{1}{G}\right). \, \mathrm{dB} \tag{8}$$

Because the noise floor of the receiver after removing the antenna gain is $-113\,\mathrm{dB}$, only the measurement points where L is smaller than $108\,\mathrm{dB}$ (another $5\,\mathrm{dB}$ is the safety margin) are considered in this work. The excess loss E of each measurement point is then obtained by using Eq. (2).

4.2. RMS Delay Spread

First, the channel impulse response $\hat{h}[t, n]$ of the tth snapshot in each measurement point is estimated from the channel transfer function [32] as

$$\hat{h}[t, n] = \frac{1}{K} \sum_{k=1}^{K} \xi \mathcal{W}[k] \hat{H}[t, k] \exp\left(j\frac{2\pi}{K}kn\right), \tag{9}$$

where $\mathcal{W}$ is a windowing function for reducing the side lobe effect in estimating $\hat{h}[i, n]$ and the correction factor $\xi = K/\sum_{k=1}^{K} \mathcal{W}[k]$. The average power delay profile $\bar{P}_{\text{h}}[n]$ of each measurement point can be obtained by

$$\bar{P}_{\text{h}}[n] = \frac{1}{T} \sum_{t=1}^{T} \left|\hat{h}[t, n]\right|^2, \tag{10}$$

To estimate the τ_{rms} in this work, as recommended in [29], the threshold for the noise exclusion is set to 20 dB from the peak of $\bar{P}_{\text{h}}[n]$. Only the measurement points where the difference between the peak and the noise level, i.e., the signal-to-noise ratio (SNR), is ≥ 25 dB, are taken into account. Finally, the τ_{rms} of each measurement point is estimated by

$$\tau_{\text{rms}} = \sqrt{\frac{\sum_{n=0}^{\text{max}} \bar{P}_{\text{h}}[n](\tau_n - \tau_{\text{mean}})^2}{\sum_{n=0}^{\text{max}} \bar{P}_{\text{h}}[n]}}, \tag{11}$$

where $\tau_n = n\Delta\tau$, $\Delta\tau$ is the delay resolution shown in Table 1, and the mean delay time τ_{mean} can be calculated as

$$\tau_{\text{mean}} = \frac{\sum_{n=0}^{\text{max}} \tau_n \bar{P}_{\text{h}}[n]}{\sum_{n=0}^{\text{max}} \bar{P}_{\text{h}}[n]}. \tag{12}$$

4.3. Coherence Bandwidth

In estimating the coherence bandwidth, only the measurement points that meet the SNR criterion described in Section 4.2 are considered. First, the normalized frequency correlation function in each measurement point is estimated [33] as

$$R_{\text{f}}[\Delta k] = \frac{\sum_{k=1}^{K-\Delta k} \sum_{t=1}^{T} \hat{H}[t, k]\hat{H}^*[t, k + \Delta k]}{\sum_{k=1}^{K-\Delta k} \sum_{t=1}^{T} |\hat{H}[t, k]|^2}. \tag{13}$$

For a particular correlation level c, typically 0.9, 0.7, and 0.5 [33, 34], the coherence bandwidth is then defined as

$$B_c = \min(\Delta k) \text{ such that } \left|R_{\text{f}}[\Delta k]\right| \leq c. \tag{14}$$

However, there is an uncertainty relationship between the RMS delay spread and the coherence bandwidth. In [35], this uncertainty relationship, called Fleury bound, was derived as

$$B_c \geq \frac{\arccos(c)}{2\pi\tau_{\text{rms}}}. \tag{15}$$

4.4. Rician K-Factor

The small-scale fading due to the superposition of multipath components can be observed in the channel transfer function $\hat{H}[t, k]$ in either the time or frequency domain [28]. When moving the Rx node or dynamic environment, this superposition over time, space, and frequency shares the same cause [28, 36] because the motion of the nodes or the scatterers causes phase shift in each multipath component. Hence, the fading statistics over time at a given frequency is similar to the statistics over frequency at any given time [28].

In this work, the Rx position was fixed for a certain static period and then moved to a new position. It can be thought as the sampling of the moving case which means that only superposition of multiple components in the frequency domain (frequency-selective fading) can be observed. Therefore, the statistics over the frequency of $\hat{H}[k]$ in each fixed location is analyzed in this paper. The main condition of the statistical modeling of the small-scale fading due to such superposition in any domain, as pointed out in [28], is that the samples in that domain have to be statistically independent random values. Thus, in the case of frequency domain, the samples have to be picked up from a bandwidth wider than the coherent bandwidth. Because the estimated $\hat{H}[t, k]$ is obtained from measurement in the time-invariant condition, the average envelope channel transfer function over the time of each measurement point represented by Eq. (16) is used:

$$\bar{H}[k] = \frac{1}{T} \sum_{t=1}^{T} \left| \hat{H}[t, k] \right|. \tag{16}$$

The frequency tones of $\bar{H}[k]$ are divided into sub-bands. Each sub-band is equivalent to the coherence bandwidth obtained from Eq. (14) using $c = 0.7$. In each sub-band, only the envelope value r of one frequency tone is regularly sampled. The probability density function (PDF) of the r values selected from $\bar{H}[k]$ of each measurement point is assumed to follow the Nakagami-Rice distribution [37] as

$$p_{\text{ric}}(r) = \frac{r}{\sigma^2} \cdot \exp\left[-\frac{(r^2 + S^2)}{2\sigma^2} \right] \cdot I_0 \left(\frac{rS}{\sigma^2} \right), \tag{17}$$

where $I_0(x)$ is the modified Bessel function of the first kind, zeroth order. The mean square value of a Nakagami-Rice distributed random variable r is given by

$$\overline{r^2} = s^2 + 2\sigma^2, \tag{18}$$

where S^2 and $2\sigma^2$ are the power contributions by the strong dominant paths and by the frequency-selective fading due to the superposition of the multipath components, respectively. The *maximum likelihood estimation* (MLE) approach is used to estimate S^2 and $2\sigma^2$. The Rician K-factor, which is the ratio of these two terms, can be calculated as

$$K_{\text{factor}} = 10 \cdot \log_{10} \left(\frac{S^2}{2\sigma^2} \right). \text{ dB} \tag{19}$$

5. PROPOSED MODELING APPROACHES

This section highlights the differences between the existing modeling approaches described in Section 2 and the alternative approaches used in this work.

5.1. The Proposed Excess Loss Model

On the basis of the measurement result which will be presented in Section 6, the number of ridges existing between the LOS of the Tx and Rx (n_{r}) is found to be the reason behind the angular variation. Therefore, the VO model is proposed to better represent such variation as

$$L_{\text{Evo}}(n_{\text{r}}) = A_{\text{vo}} \left\{ 1 - \exp\left(-\frac{R_{\text{vo}}}{A_{\text{vo}}} n_{\text{r}} \right) \right\}. \text{ dB} \tag{20}$$

where R_{vo} and A_{vo} are the initial gradient of the attenuation rate of E over n_{r} and the maximum of E, respectively.

5.2. Model Selection

In this work, the results of E obtained using Eq. (2) are fitted with the empirical distance-dependent model $L_\text{E}(d)$ in the following form,

$$E(d) = L_\text{E}(d) + X, \ \text{dB} \tag{21}$$

where $X \sim N(0, \sigma^2)$ can be generally assumed to be a normal distributed random variable with zero mean and variance σ^2. To avoid the drawback of the existing approach described in Section 2.2, this paper utilizes an appropriate approach which uses the Akaike information criterion (AIC) [38] where the number of model parameters m is also taken into account. The general form of AIC is expressed as

$$\text{AIC} = -2\log(\mathcal{L}(\hat{\Theta}|\mathbf{y})) + 2m, \tag{22}$$

where $\mathbf{y} = [y_1, y_2, \ldots, y_s]$ is the sample's vector, $\hat{\Theta} = [\theta_1, \theta_2, \ldots, \theta_m]$ the parameters of the model, and $\mathcal{L}(\hat{\Theta}|\mathbf{y})$ the *likelihood function*.

If the statistical model is appropriated to represent the channel parameters, the general form of AIC in Eq. (22) is directly used. For the least squares fitting problem of Eq. (21), the AIC was derived and presented in [39, pp. 63] as

$$\text{AIC} = s\log(\hat{\sigma}^2) + 2m, \tag{23}$$

where s denotes the sample size, and $\hat{\sigma}^2$ is the maximum likelihood estimate of σ^2 and represented by

$$\hat{\sigma}^2 = \frac{\sum \hat{X}_d^2}{s}, \tag{24}$$

where $\hat{X}_d$ is the estimated X indexed by the vegetation depth d for a particular candidate model.

When the ratio s/m is small (say < 40) [39, pp. 66], the second-order variant of AIC called AIC_c, which was derived by [40] and represented by Eq. (25), should be used as the model selection criterion.

$$\text{AIC}_\text{c} = \text{AIC} + \frac{2m(m+1)}{s - m - 1}. \tag{25}$$

5.3. Small-Scale Fading Modeling

In this work, the small-scale fading in the tall food grass field at a vegetation depth $d < 40\,\text{m}$ is modeled by the K-factor of the Nakagami-Rice distribution. The relationship between the Rician K-factor and other environmental factors — not only d — is investigated. In addition, as explained in Section 7, the relationship between the small-scale fading parameter over the path loss value L is confirmed and modeled.

5.4. Wideband Characteristic Modeling

The RMS delay spread τ_rms in the tall food grass field at $d < 40\,\text{m}$ is modeled. The dependence of τ_rms on d and other environmental factors is confirmed by the hypothesis test. If the dependency hypothesis is rejected, the statistical model is proposed to represent the randomness of the τ_rms values. In such a case, the selection criterion of the statistical model expressed as Eq. (22) is applied.

6. PATH LOSS

The results of the excess loss E obtained using Eq. (2) in the sugarcane field are presented in Fig. 4. Such E values of the measurement points in each angular direction are fitted by the MA model expressed as Eq. (4) which gives the lowest AIC_c values obtained by Eqs. (23) and (25) among the MED, MA, and ZNG models presented in Section 2.1.2. The variation in the two parameters of the MA model, A_m and R_0, over the angular directions is shown in Fig. 5. It is obvious that the excess loss E increases when the angle increases. However, it is not significantly different for some angles such as $20°$ and $30°$, as well as for $70°$, $80°$ and $90°$. Considering two parameters of the MA model, A_m shows a similar level of approximately $40\,\text{dB}$ in every angular direction except $0°$, while R_0 is dependent on the angular direction. Therefore, R_0 which represents the loss rate in the shorter vegetation depth is the major
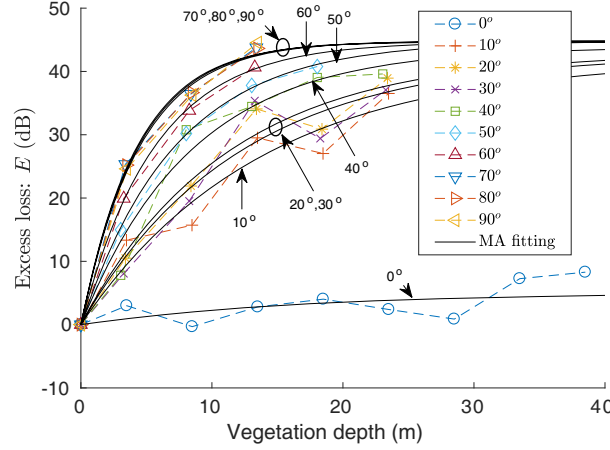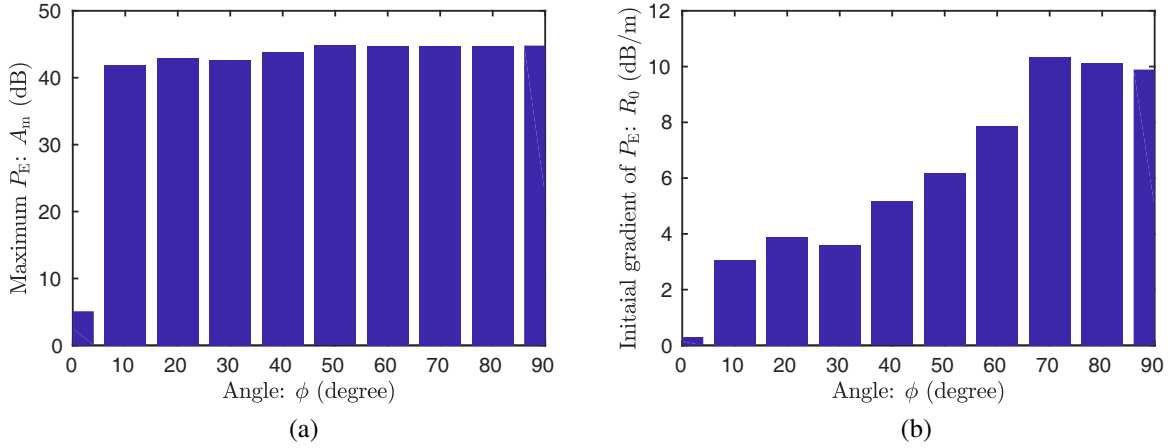
Figure 4. Excess loss values fitted with the MA model.

Figure 5. Parameters of the MA model in sugarcane field: (a) A_{m}. (b) R_0.

cause of the variation over the angular directions. However, similar values of R_0 can be observed in some consecutive angles. The reason for this angular variation will be presented in the next subsection. Furthermore, a comparison with the parameters of the MA model in the forest/woodland that was extensively reported in [11] shows that the R_0 values in this agriculture field are significantly greater except in the 0° direction.

6.1. Angular Variation

Considering the sugarcane planting pattern shown in Fig. 3, the major factor that makes the difference in each measurement direction is the number of ridges between the LOSs of the Tx and Rx defined as n_{r}. In Fig. 6(a), d and n_{r} of each measurement point in each angular direction are shown. Obviously, the similar E and R_0 values in 20° and 30° are because they have the same n_{r}. This is also the case with 70°, 80° and 90°. The plot of E values in all angular directions versus n_{r} is presented in Fig. 6(b). They can be represented well by the VO model described in Subsection 5.1:

$$L_{\mathrm{Evo}}(n_{\mathrm{r}}) = 42.9 \left\{ 1 - \exp\left(-\frac{15.8}{42.9} n_{\mathrm{r}} \right) \right\}. \, \mathrm{dB} \tag{26}$$

This model also exhibits two gradients of the attenuation rate: the greater rate at smaller n_{r} and the smaller rate at larger n_{r}. Because n_{r} represents the magnitude of the vegetation length, which is analogous to the vegetation depth d, the VO model in Eq. (26) can also be described by the interplay
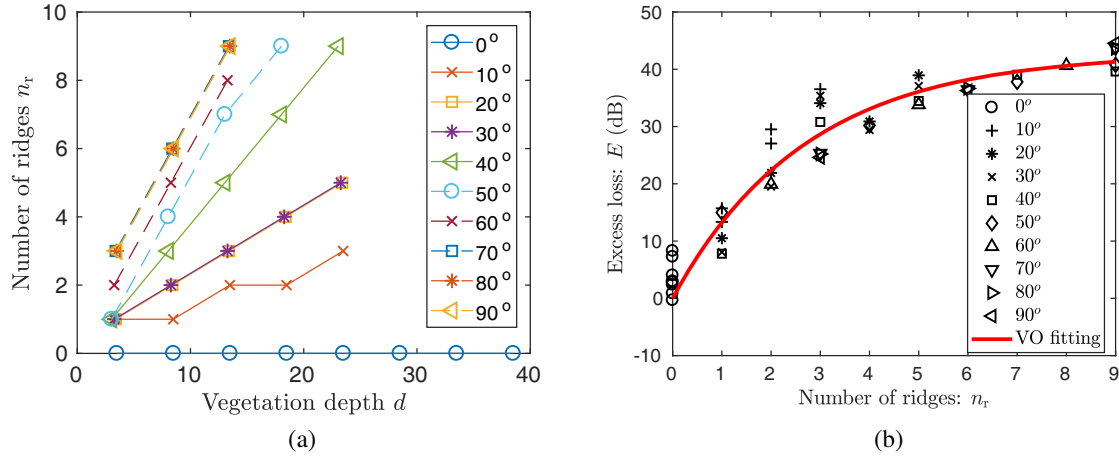
Figure 6. (a) Vegetation depth d and the number of ridges between LOS of Tx and Rx $n_{\rm r}$ of each measurement point, (b) excess loss values E fitted by the VO model.

of the coherent and incoherent components of radio propagation in the vegetation medium as explained in Section 2.1.1. From this result, it can be concluded that the different values of $n_{\rm r}$ in each angular direction are the main reason for the angular excess loss variation. $n_{\rm r}$ increases when the angle increases, causing the strong angular dependence described previously. Note that with the ridge width at 0.15 m as described in Section 3, the vegetation length of each ridge in each angle is not significantly different.

6.2. Procedure of Predicting the Path Loss at Any Point in the Tall Food Grass Field

The finding explained previously provides a way of predicting the attenuation at any point in the field by using a few measurement efforts. This knowledge is useful for practical WSN planning and management. The procedure can be described as follows:

- The first step is to obtain the results of the excess loss E in only one direction, e.g., 90°, by either dedicated measurement or derivation of the values on the basis of the received signal strength indication (RSSI) collected from the existing wireless sensor nodes in the field.
- Second, the VO model $L_{\rm Evo}(n_{\rm r})$ expressed as (26) is applied by fitting the obtained results of E over $n_{\rm r}$. From the measurement result described previously, this $L_{\rm Evo}(n_{\rm r})$ can be applied to any angle.
- Finally, using d and $n_{\rm r}$, the path loss at any point can be predicted by

$$L_{\rm L}(d, n_{\rm r}) = L_{\rm F}(d) + L_{\rm Evo}(n_{\rm r}). \text{ dB} \tag{27}$$

The proposed prediction procedure assumes the following conditions:

- The crops have the same age of growth. Therefore, the leaf size and stalk size are not significantly different over the crops.
- The crops are planted and distributed closely in a narrow ridge pattern. Such characteristics should follow the main assumption such that the vegetation length of each ridge in each angle is not significantly different.
- The crops must be higher than the antenna height.

Although further experimental validation is needed, the same procedure is expected to be applicable to other food grass agriculture fields under the above conditions.

7. SMALL-SCALE FADING

As explained in Section 4.4, the Rician K-factor is used to represent the small-scale fading due to the superposition of multipath components. Furthermore, the SNR criterion described in Section 4.2 is
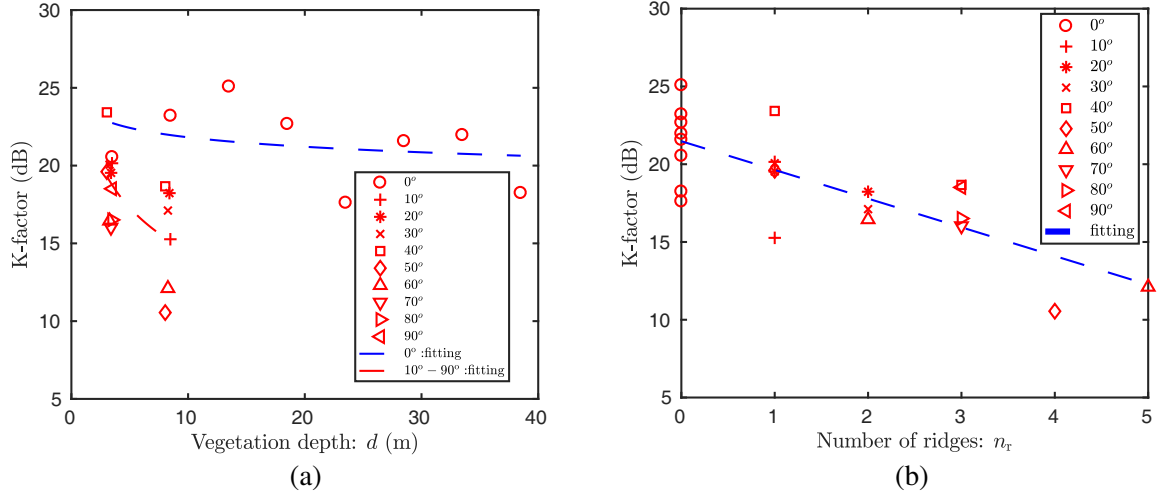
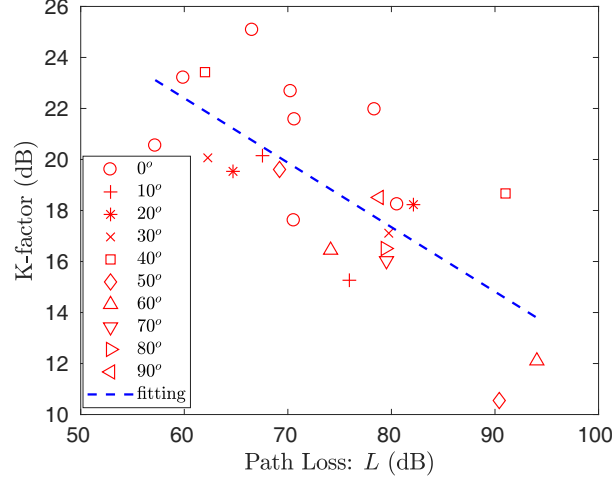**Figure 7.** The plot of K-factor. (a) Over d and (b) over n_{r}.

Figure 8. Relationship between the K-factor and its corresponding path loss value L of each measurement point.

applied to estimate B_c defined in Eq. (14), which is then used to estimate K-factor as explained in Section 4.4. Therefore, the results of some measurement points are excluded. From now, when the term K-factor is stated, it means the Rician K-factor in dB.

Considering the d dependence of the K-factor in Fig. 7(a), the different log-linear relationships between $0°$ and other directions can be observed because there exists a small number of multipath components due to a few obstructions in $0°$. On the other hand, considering n_{r}, which represents the level of obstructions, as shown in Fig. 7(b), the K-factor values in all directions can be fitted by a single model. Note that the fitting line shown in Fig. 7(b) is linear, not log-linear, because $n_{\mathrm{r}} = 0$ in $0°$ and $\log_{10}(0)$ cannot be determined.

However, considering the physical mechanism of the multipath components due to the signal reflections in the tall food grass field, the variation in the K-factor may not be caused by only an individual factor but by the combination of both d and n_{r} factors. Because the path loss is also the function of these two factors as shown in Eq. (27), the relationship between the K-factor and its corresponding path loss value L of each measurement point is examined and presented in Fig. 8. This relationship can be represented as

$$K_{\mathrm{factor}}(L) = 37.58 - 0.25L + N(0, 2.41), \tag{28}$$

where L is in dB, and the last term $N(0, \sigma)$ represents the normally distributed random variable with zero mean and standard deviation σ. In regard to the measurement results of a suburban non-LOS microcellular environment in [41], the relationship between the K-factor and L was also observed. This result suggests that it might be possible to predict the K-factor at any point in the field if the path loss information is available.

8. WIDEBAND CHARACTERISTIC

The RMS delay spread, τ_{rms}, of each measurement point is estimated by the approach described in Section 4.2. Such values are plotted over d and n_{r} as shown in Fig. 9. Note that the results of some measurement points are excluded due to the SNR criterion described in Section 4.2. The dependence of τ_{rms} on these two factors cannot be clearly observed. Statistically, the Pearson's correlation coefficient [42, pp. 331] between τ_{rms} and d, and between τ_{rms} and n_{r} are -0.112 and 0.405, respectively. By using the hypothesis test (t-test) for zero correlation described in [42, pp. 333], the hypothesis of lack of association is accepted at a significance level (α) of 0.05 with p-values 0.612 and 0.055 for d and n_{r}, respectively.

On the basis of randomness, the τ_{rms} parameter is modeled by the statistical distribution in this work. The AIC defined as Eq. (22) is used as the criterion to select the best model among six well-known probability models: Gaussian, Gamma, Nakagami-m, Nakagami-Rice, Rayleigh, and Weibull. Consequently, the Weibull distribution which gives the lowest AIC value is used to model the τ_{rms}
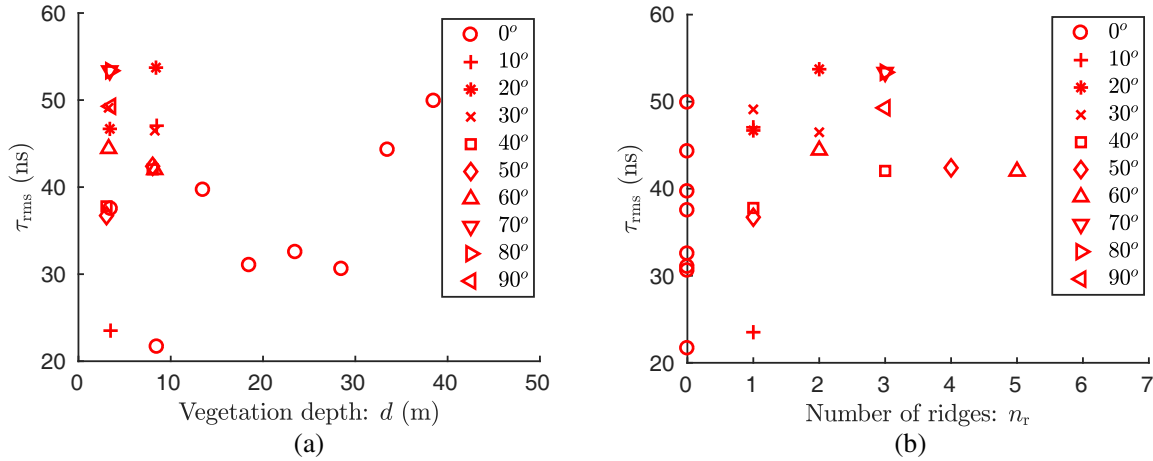

Figure 9. The plot of τ_{rms} over (a) d factor and (b) n_{r} factor.
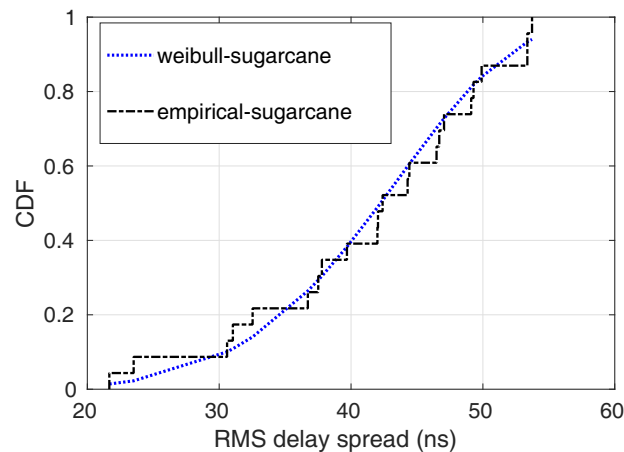

Figure 10. Empirical CDF of τ_{rms} and its corresponding Weibull CDF.

parameter in this case. The PDF of the fitted Weibull model is expressed as

$$p_{\text{wei}}(\tau_{\text{rms}}) = \begin{cases} \dfrac{b}{a}\left(\dfrac{\tau_{\text{rms}}}{a}\right)^{b-1} \exp\left(-(\dfrac{\tau_{\text{rms}}}{a})^b\right), & \tau_{\text{rms}} \geq 0 \\ 0, & \tau_{\text{rms}} < 0 \end{cases} \tag{29}$$

where the a and b parameters are 44.98 and 5.83, respectively. The empirical cumulative density function (CDF) of τ_{rms} and its corresponding Weibull CDF are shown in Fig. 10.

9. CONCLUSION

This paper describes the radio wave propagation measurement campaign and characterization in a sugarcane field representing tall food grass which is one of the common types of agricultural environment. The measurement was conducted by using a channel sounder having a bandwidth of 45.6 MHz at 2.45 GHz. The location of the Tx was fixed, and then the Rx was moved over a vegetation depth d and angular direction ϕ. Unlike other works, this measurement setting allows the study of not only the d-dependent excess loss but also the variation in the excess loss over ϕ. In addition, the vegetation depth range d in this measurement was shorter than 40 m, which is more applicable to the WSN in the precision agriculture application than the ranges employed in the existing works. The conclusions and significant observations of the measurement results are summarized as follows:

- The results of the excess loss E were fitted well with the MA model, and the model's parameter is strongly dependent on ϕ.
- While the numbers of ridges n_{r} are different in most ϕ, the same relationship between E and n_{r} exists in every ϕ. In other words, n_{r} is the reason for the angular dependence excess loss.
- The VO model as a function of one parameter (n_{r}) instead of two parameters $(d$ and $\phi)$ is proposed to better represent the excess loss E.
- The prediction procedure of the path loss at any point in the field that employs a few measurement efforts was proposed on the basis of the above finding.
- The relationship between the Rician K-factor and its corresponding path loss value L in each measurement point could be fitted with the log-linear line. This suggests the possibility of predicting the K-factor at any point in the field if the path loss information is available.
- The results of the RMS delay spread are independent of d and n_{r}. Therefore, they are represented by a statistical model. The Weibull distribution was chosen as it gives the best representation.

REFERENCES

1. Bongiovanni, R. and J. Lowenberg-Deboer, "Precision agriculture and sustainability," *Precision Agriculture*, Vol. 5, No. 4, 359–387, Aug. 2004.
2. Ndzi, D. L., A. Harun, F. M. Ramli, M. L. Kamarudin, A. Zakaria, A. Y. M. Shakaff, M. N. Jaafar, S. Zhou, and R. S. Farook, "Wireless sensor network coverage measurement and planning in mixed crop farming," *Computers and Electronics in Agriculture*, Vol. 105, 83–94, 2014.
3. Srisooksai, T., K. Keamarungsi, P. Lamsrichan, and K. Araki, "Practical data compression in wireless sensor networks: A survey," *Journal of Network and Computer Applications*, Vol. 35, No. 1, 37–59, Jan. 2012.
4. Castiglione, P., S. Savazzi, M. Nicoli, and T. Zemen, "Partner selection in indoor-to-outdoor cooperative networks: An experimental study," *IEEE Journal on Selected Areas in Communications*, Vol. 31, No. 8, 1559–1571, Aug. 2013.

5. Savage, N., D. Ndzi, A. Seville, E. Vilar, and J. Austin, "Radio wave propagation through vegetation: Factors influencing signal attenuation," *Radio Science*, Vol. 38, No. 5, n/a–n/a, Oct. 2003.

6. Joshi, G. G., C. B. Dietrich, C. R. Anderson, W. G. Newhall, W. A. Davis, J. Isaacs, and G. Barnett, "Near-ground channel measurements over line-of-sight and forested paths," *IEE Proceedings — Microwaves, Antennas and Propagation*, Vol. 152, No. 6, 589–596, Dec. 2005.

7. Gay-Fernandez, J. A., M. Garcia Sánnchez, I. Cuinas, A. V. Alejos, J. G. Sanchez, and J. L. Miranda-Sierra, "Propagation analysis and deployment of a wireless sensor network in a forest," *Progress In Electromagnetics Research*, Vol. 106, 121–145, 2010.

8. Gay-Fernández, J. A. and I. Cuiñas, "Peer to peer wireless propagation measurements and path-loss modeling in vegetated environments," *IEEE Transactions on Antennas and Propagation*, Vol. 61, No. 6, 3302–3311, Jun. 2013.

9. Oestges, C., B. M. Villacieros, and D. Vanhoenacker-Janvier, "Radio channel characterization for moderate antenna heights in forest areas," *IEEE Transactions on Vehicular Technology*, Vol. 58, No. 8, 4031–4035, Oct. 2009.

10. Gay-Fernández, J. A. and I. Cuiñas, "Short-term modeling in vegetation media at wireless network frequency bands," *IEEE Transactions on Antennas and Propagation*, Vol. 62, No. 6, 3330–3337, Jun. 2014.

11. ITU-R P.833-9, "Attenuation in vegetation," Sep. 2016.

12. Anderson, C. R., H. I. Volos, and R. M. Buehrer, "Characterization of low-antenna ultrawideband propagation in a forest environment," *IEEE Transactions on Vehicular Technology*, Vol. 62, No. 7, 2878–2895, Sep. 2013.

13. Grivet, L. and P. Arruda, "Sugarcane genomics: Depicting the complex genome of an important tropical crop," *Current Opinion in Plant Biology*, Vol. 5, No. 2, 122–127, 2002.

14. Balachander, D., T. R. Rao, and G. Mahesh, "RF propagation experiments in agricultural fields and gardens for wireless sensor communications," *Progress In Electromagnetics Research C*, Vol. 39, 103–118, 2013.

15. Ndzi, D. L., L. M. Kamarudin, A. A. Muhammad Ezanuddin, A. Zakaria, R. B. Ahmad, M. F. B. A. Malek, A. Y. M. Shakaff, and M. Jafaar, "Vegetation attenuation measurements and modeling in plantations for wireless sensor network planning," *Progress In Electromagnetics Research B*, Vol. 36, 283–301, 2012.

16. Hara, M., H. Shimasaki, Y. Kado, and M. Ichida, "Effect of vegetation growth on radio wave propagation in 920-MHz band," *IEICE Transactions on Communications*, Vol. 99, No. 1, 81–86, 2016.

17. Amaral, L. R., R. G. Trevisan, and J. P. Molin, "Canopy sensor placement for variable-rate nitrogen application in sugarcane fields," *Precision Agriculture*, Vol. 19, No. 1, 147–160, Feb. 2018.

18. Garcia-Sanchez, A.-J., F. Garcia-Sanchez, and J. Garcia-Haro, "Wireless sensor network deployment for integrating video-surveillance and data-monitoring in precision agriculture over distributed crops," *Computers and Electronics in Agriculture*, Vol. 75, No. 2, 288–303, 2011.

19. Payne, A. B., K. B. Walsh, P. P. Subedi, and D. Jarvis, "Estimation of mango crop yield using image analysis — Segmentation method," *Computers and Electronics in Agriculture*, Vol. 91, 57–64, 2013.

20. Cubero, S., W. S. Lee, N. Aleixos, F. Albert, and J. Blasco, "Automated systems based on machine vision for inspecting citrus fruits from the field to postharvest — A review," *Food and Bioprocess Technology*, Vol. 9, No. 10, 1623–1639, 2016.

21. IEEE Std 802.15.4-2015 (Revision of IEEE Std 802.15.4-2011), "IEEE standard for low-rate wireless networks," IEEE 2006, Apr. 2016.

22. Meng, Y. S. and Y. H. Lee, "Investigations of foliage effect on modern wireless communication systems: A review," *Progress In Electromagnetics Research*, Vol. 105, 313–332, 2010.

23. Johnson, R. and F. Schwering, "A transport theory of millimeter wave propagation in woods and forests," US Army, Comumunications-Electronics Command, Fort Monmouth, New Jersey, Tech.

Rep. CECOM-TR-85-1, 1985.

24. COST 235 Management Committee, COST 235 Radiowave Propagation Effects on Nextgeneration Fixed-Services Terrestrial Telecommunications Systems, 1996.

25. Seville, A. and K. H. Craig, "Semi-empirical model for millimetre-wave vegetation attenuation rates," *Electronics Letters*, Vol. 31, No. 17, 1507–1508, Aug. 1995.

26. Al-Nuaimi, M. and A. Hammoudeh, "Measurements and predictions of attenuation and scatter of microwave signals by trees," *IEE Proceedings-Microwaves, Antennas and Propagation*, Vol. 141, No. 2, 70–76, 1994.

27. Meng, Y. S., Y. H. Lee, and B. C. Ng, "Empirical near ground path loss modeling in a forest at VHF and UHF bands," *IEEE Transactions on Antennas and Propagation*, Vol. 57, No. 5, 1461–1468, May 2009.

28. Kattenbach, R., "Statistical modeling of small-scale fading in directional radio channels," *IEEE Journal on Selected Areas in Communications*, Vol. 20, No. 3, 584–592, Apr. 2002.

29. ITU-R P.1407-5, "Multipath propagation and parametrization of its characteristics," Sep. 2013.

30. Srisooksai, T., J. Takada, and K. Saito, "Portable wide-band channel sounder based software defined radio for studying the radio propagation in an outdoor environment," *2017 International Symposium on Antennas and Propagation (ISAP)*, 1–2, Oct. 2017.

31. Kaemarungsi, K., "Development and deployment of ZigBee wireless sensor networks for precision agriculture in sugarcane field," *Asia-Pacific Advanced Network (APAN) 33rd*, Feb. 2012.

32. Kim, M., Y. Konishi, Y. Chang, and J. Takada, "Large scale parameters and double-directional characterization of indoor wideband radio multipath channels at 11 GHz," *IEEE Transactions on Antennas and Propagation*, Vol. 62, No. 1, 430–441, Jan. 2014.

33. Al-Nuaimi, M. O. and A. G. Siamarou, "Coherence bandwidth characterisation and estimation for indoor Rician multipath wireless channels using measurements at 62.4 GHz," *Antennas and Propagation IEE Proceedings — Microwaves*, Vol. 149, No. 3, 181–187, Jun. 2002.

34. Varela, M. S. and Sanchez, M. G., "RMS delay and coherence bandwidth measurements in indoor radio channels in the UHF band," *IEEE Transactions on Vehicular Technology*, Vol. 50, No. 2, 515–525, Mar. 2001.

35. Fleury, B. H., "An uncertainty relation for WSS processes and its application to WSSUS systems," *IEEE Transactions on Communications*, Vol. 44, No. 12, 1632–1634, Dec. 1996.

36. Oestges, C., N. Czink, B. Bandemer, P. Castiglione, F. Kaltenberger, and A. J. Paulraj, "Experimental characterization and modeling of outdoor-to-indoor and indoor-to-indoor distributed channels," *IEEE Transactions on Vehicular Technology*, Vol. 59, No. 5, 2253–2265, Jun. 2010.

37. Molisch, A. F., *Wireless Communications*, 2nd edition, John Wiley & Sons, 2011.

38. Akaike, H., "Information theory and an extension of the maximum likelihood principle," *Selected Papers of Hirotugu Akaike*, E. Parzen, K. Tanabe, and G. Kitagawa (eds.), 199–213, Springer, New York, NY, New York, 1998.

39. Burnham, K. P., D. R. Anderson, and K. P. Burnham, *Model Selection and Multimodel Inference: A Practical Information-Theoretic Approach*, 2nd edition, Springer, New York, 2002.

40. Sugiura, N., "Further analysts of the data by akaike's information criterion and the finite corrections: Further analysts of the data by akaike's," *Communications in Statistics — Theory and Methods*, Vol. 7, No. 1, 13–26, Jan. 1978.

41. Takada, J., J. Fu, H. Zhu, and T. Kobayashi, "Spatio-temporal channel characterization in a suburban non line-of-sight microcellular environment," *IEEE Journal on Selected Areas in Communications*, Vol. 20, No. 3, 532–538, Apr. 2002.

42. Walpole, R. E., Ed., *Essentials of Probability and Statistics for Engineers and Scientists*, Pearson, Boston, Mass., 2013.